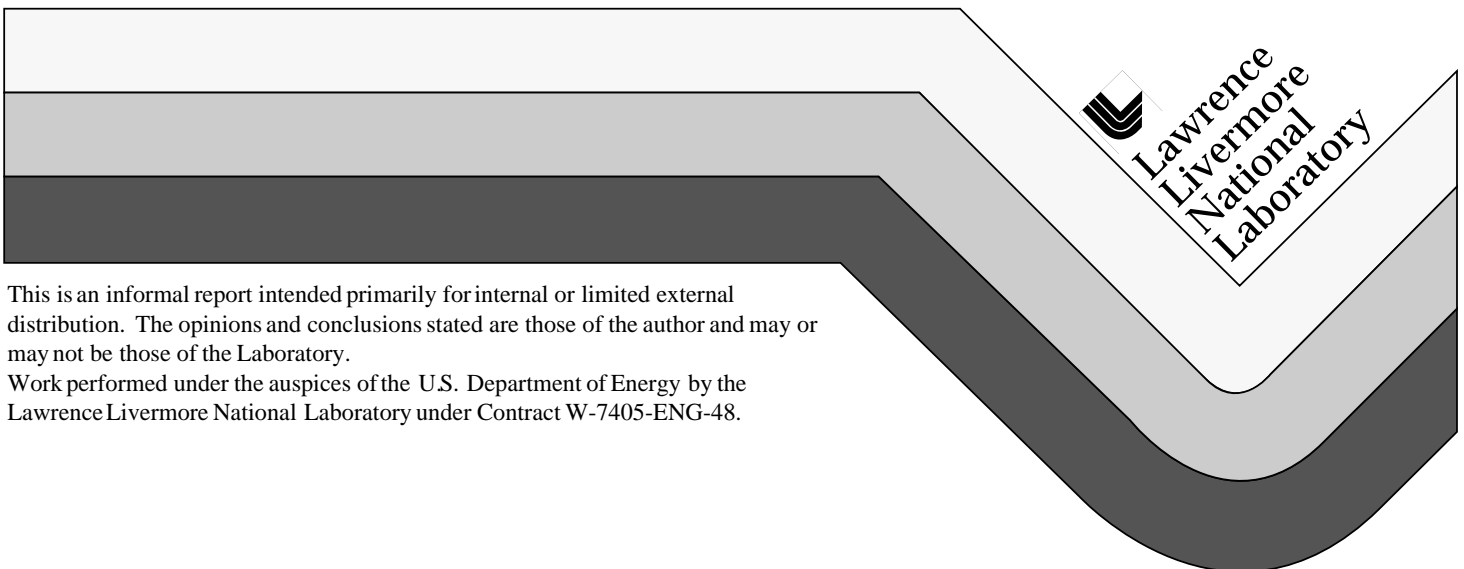# Determination of Mineral Abundances in Samples from the Exploratory Studies Facility Using X-Ray Diffraction

Sarah Roberts
Brian Viani

January 13, 1998

Lawrence Livermore National Laboratory

DISCLAIMER

This document was prepared as an account of work sponsored by an agency of the United States Government. Neither the United States Government nor the University of California nor any of their employees, makes any warranty, express or implied, or assumes any legal liability or responsibility for the accuracy, completeness, or usefulness of any information, apparatus, product, or process disclosed, or represents that its use would not infringe privately owned rights. Reference herein to any specific commercial product, process, or service by trade name, trademark, manufacturer, or otherwise, does not necessarily constitute or imply its endorsement, recommendation, or favoring by the United States Government or the University of California. The views and opinions of authors expressed herein do not necessarily state or reflect those of the United States Government or the University of California, and shall not be used for advertising or product endorsement purposes.

This report has been reproduced
directly from the best available copy.

Available to DOE and DOE contractors from the
Office of Scientific and Technical Information
P.O. Box 62, Oak Ridge, TN 37831
Prices available from (423) 576-8401

Available to the public from the
National Technical Information Service
U.S. Department of Commerce
5285 Port Royal Rd.,
Springfield, VA 22161

**Determination of Mineral Abundances in Samples from the Exploratory Studies
Facility Using X-ray Diffraction**

Deliverable SPY195M4

January 13, 1998

Sarah Roberts and Brian Viani

Geosciences and Environmental Technologies Division
Lawrence Livermore National Laboratory

Introduction

Tuff samples collected from the Exploratory Studies Facility (ESF) were X-rayed to
estimate relative mineral abundances. X-ray analysis was performed on sub-samples
of specimens collected from both the Single Heater Test (SHT) and Drift Scale Heater
Test (DST) that were used for thermomechanical measurements, as well as samples
collected from cores retrieved from boreholes in the Drift Scale Test Area. The
abundance of minerals that could affect the behavior of the host rock at repository
relevant temperatures is of particular interest. These minerals include cristobalite,
which undergoes a phase transition and volume change at elevated temperature
(~250 °C), and smectite and clinoptilolite that can dehydrate at elevated temperature
with accompanying volume reduction. In addition, the spatial distribution of SiO_2
polymorphs and secondary minerals may provide evidence for deducing past fluid
pathways. The mineral abundances tabulated here include data reported previously
in three milestone reports (Roberts and Viani, 1997a,b; Viani and Roberts, 1996) but
re-analyzed (see below), as well as previously unreported data.

Previous X-ray diffraction analyses of samples from the ESF (Roberts and Viani,
1997a; Viani and Roberts, 1996) utilized the matrix flushing method of Chung (1974)
and an internal intensity standard (corundum) to quantify the abundances of the
phases present. Although the method is adequate for obtaining relative
abundances, its accuracy and precision is limited by the inherent differences between
the external standards used to compute the reference intensity ratio and the mineral
phases in the sample. In a subsequent report (Roberts and Viani, 1997b) mineral
abundances were obtained using the Rietveld method of whole X-ray pattern fitting
(Snyder and Bish, 1989; Young, 1993). The Rietveld technique has the potential to be
both more accurate and more precise for estimating mineral abundances (Snyder
and Bish, 1989).

The mineral abundances originally determined using the matrix flushing method
(Viani and Roberts, 1996; Roberts and Viani, 1997a) have been re-determined using
the Rietveld method using the original X-ray data and are reported in Tables 1 and 2.
In addition, mineral abundances determined using the Rietveld method (Roberts
and Viani; 1997b) were also re-analyzed using the optimized Rietveld parameters
used to re-analyze the earlier data sets (Table 3). Finally, X-ray diffraction data for

DST drillcore samples not reported in the earlier reports were also analyzed using the Rietveld method (Table 2). The data presented in Tables 1-3 represent our best estimates of mineral abundances for the listed samples. This data supercedes the mineral abundances previously reported in Roberts and Viani (1997a,b) and Viani and Roberts (1996).

In addition to the samples analyzed for abundance, a suite of accompanying fracture and cavity fill minerals was also analyzed to identify the phases present. The results of these analyses are shown in Table 4.

Method

The Rietveld method is based on fitting a calculated X-ray diffraction (XRD) pattern to the observed pattern over the entire angular range over which data is collected. The calculated pattern is refined by adjusting the quantity of the phases included in the calculation (scale factor), as well as their crystallographic properties. The Rietveld method of quantification avoids the use of external standards. The method requires identification of all the phases in the sample, as the refined abundances are normalized to 100%. In order to assess the overall accuracy of the method, a known quantity of corundum was added to each sample.

Mineral quantification using the Rietveld method involved two steps. First, the phases present in each sample were identified using an XRD pattern processing software program (Jade, version 3.0, Materials Data, Inc., Livermore, CA), which utilizes data from the Joint Committee on Powder Diffraction Standards Powder Diffraction File (JCPDS-PDF). After the mineral phases were identified, the Rietveld method of quantification was employed. A least squares refinement is carried out until the best fit is obtained between the observed powder diffraction pattern and the calculated pattern based on the crystal structures and lattice parameters of phases determined to be present. The Rietveld analyses were performed using a quantitative XRD software program (Siroquant, version 2.0, Sietronics, Australia).

Sample and standard preparation

All samples were crushed using an hydraulic press to <1/4-inch, then processed through a flat-plate pulverizer until the entire sample passed a 250-µm sieve. A sub-sample of each was then further ground in a vibratory micro-mill (Fritsch) with a sintered corundum mortar and ball for 60 minutes at ~1/3 full power using an intermittent power cycle. Standard mineral specimens were crushed by hand, if necessary, and then ground in the micro-mill in the same fashion as the tuff samples. Accompanying fracture minerals were hand picked out of the cores and ground as described above. The particle sizes of the milled samples and standards were checked using an optical microscope. Particle sizes determined by this method were approximately 10 µm or less. The corundum internal standard (Buehler, 1.0-µm Al_2O_3) was not ground because of its small size. The ground samples were mixed with corundum in a 4:1 ratio, and again placed in the micro-mill for 30 minutes

using the power cycles described above. Samples were packed into stainless steel side-mount holders having a sample length of 18 mm and width of 13 mm.

Sub-samples from specimens used for SHT and DST thermomechanical tests (Tables 1 and 3) were ground and homogenized; that is, there was no attempt to sample these on the basis of morphology. In contrast, the samples collected from DST drillcore (Table 2) were sampled on the basis of color variation. Three distinct colors were observed: dark purple and brown zones in the matrix, and gray zones adjacent to lithophysae and fractures. To determine if a mineralogical difference existed between the three matrix types, samples of each of these were selected for X-ray analysis. The sampling protocol consisted of examining each core sample individually and choosing either one or two of the matrix types for analysis.

X-ray diffractometer instrumental parameters

X-ray scans were collected using a Scintag PAD-V generator equipped with a Cu X-ray tube operated at 45 kV and 35 mA, and a Sieffert goniometer with a solid-state detector. Diffraction patterns were collected in step scan mode at 2 seconds per 0.02° 2θ. Collimation was provided by a 1° divergence and 2° scatter slit on the X-ray tube and a 0.3-mm scatter and 0.2-mm registration slit on the detector. Samples were scanned from 2-52°, 2-72°, or 2-82° 2θ.

Calibration correction

Prior to mineral phase identification and Rietveld analysis, the observed diffraction pattern was corrected for instrumental error based on a calibration curve determined using standard phases. The calibration correction used to correct data for this report was derived by scanning two standards; a fluorophlogopite mica for the low angle peaks (NIST traceable), and a mixture of silicon (NIST traceable), tungsten, and silver metals (SiWAg) for the high angle peaks. Both standards were scanned with the same instrumental parameters listed in the above section, the mica from 2-72° 2θ; and the SiWAg from 20-110° 2θ. The two scans were merged into one and a calibration curve built on observed versus the NIST and JCPDS-PDF 2θ angles.

Identification of mineral phases present

The Jade pattern-processing program was used to identify major and minor mineral phases present in each sample. The Jade program searches located peaks only, and compares them with the strongest lines of a potential phase in the PDF database. The selected peaks are checked visually to confirm realistic phase identification.

Rietveld quantitative analysis parameters

To calculate (or refine) an XRD pattern, Siroquant uses crystallographic information from its database, and refines these default values to achieve a good fit to the observed data. The program refines the most important parameters first, and then progresses to secondary parameters. This produces an optimum fit and the most

accurate quantification of the abundances. For this report, all XRD patterns were analyzed using the same refinement parameters. These parameters, obtained after trying a variety of refinement procedures, produced the best estimate for the abundance of the corundum internal standard (20% by weight).

The X-ray analyses from previous reports (Viani and Roberts, 1996; Roberts and Viani, 1997a,b), and new data not previously reported, have been analyzed according to the following procedure. Background is removed from the observed XRD diffraction pattern and a task is produced which specifies which mineral phases are to be included in the model. The calculated XRD pattern is then refined by varying the following parameters in the following order:

- Scale (i.e., abundance of each identified phase)
- Instrument zero
- Peak width factor (W)
- Unit cell dimensions (a,b,c) (dependent on phase)

Each set of refinement parameters was refined for 10 cycles with a damping factor of 0.2 to reduce parameter oscillations. Additional refinement cycles were performed if chi-squared (error associated with refinement parameters) for any phase did not indicate a good fit. Refinement was terminated when chi-squared had reached its lowest level for all phases. The output from Siroquant consists of the abundances of the identified phases (including the corundum internal standard) normalized to 100%. For the three data sets tabulated the average value of the corundum abundance varied between 20.6 and 22%. The mineral abundances reported in Tables 1-3 have been re-normalized on a corundum-free basis.

Comparison of most recent analysis of mineral abundances with previous results

Figures 1 and 2 compare the abundance of quartz and cristobalite determined previously using the matrix flushing method (but normalized to 100% for comparison to current results) to the mineral abundances calculated using the optimized Rietveld method described above. For quartz and cristobalite, both methods result in similar estimates of their abundance. In contrast, the estimates of abundances of individual feldspar phases differ significantly (not shown), but the estimates of total feldspar abundances are similar for each method. We attribute the discrepancy in feldspar abundances to the difficulty of using the matrix flushing method to estimate abundances for these chemically variable minerals (Vaniman et al., 1996; Roberts and Viani, 1997a).

The greatest difference between the two methods is in the estimate of the abundance of smectite. The Rietveld method consistently returned abundance values near zero for samples in which smectite was identified and for which the matrix flushing method produced values between 1 and 5%. The smectite abundances estimated using the matrix flushing method are similar to smectite values reported in Vaniman et al. (1996) for Topopah Spring tuff samples. However, we believe that, aside from the discrepancies in the smectite abundances, mineral abundances

estimated using the Rietveld approach are not only more easily obtained, but are more accurate and precise.

Re-analysis of the DST drillcore data from Roberts and Viani (1997a) resulted in the identification of stellerite in one sample that had not been identified previously. An additional sample containing stellerite was noted in a sample analyzed subsequent to Roberts and Viani's (1997a) report.

Results and Discussion

Except for one sample containing 12% zeolite (stellerite), SiO_2 polymorphs and feldspars comprise ≥95% by weight of the samples analyzed (Tables 1-3). Small amounts of mica, smectite, clinoptilolite, and stellerite were measured in roughly a quarter of the samples. The total abundance of SiO_2 polymorphs and feldspars is quite uniform, averaging between 30.5 and 34.5%, and 65.4 and 67.1%, respectively, for the three data sets. As might be expected, the data for the homogenized samples (thermal test specimens for the SHT and DST; Tables 1 and 3) show less variability than the data for samples collected from the DST drillcore on the basis of color (Table 2). The observed uniformity in total SiO_2 polymorphs and total feldspar abundances is consistent with the highly uniform chemical composition of these rocks (Schuraytz et al., 1986; Vaniman et al., 1996).

The uniformity of total SiO_2 polymorphs and total feldspar abundances were also noted by Vaniman et al. (1996) for the Topopah Spring. However, the average abundances reported here, differ from the abundances reported by Vaniman et al. (1996) for a relatively densely spaced set of core samples (UE-25 UZ#16) taken from the upper lithophysal to lower lithophysal units of the Topopah Spring (~139-329 m). Vaniman et al. report higher abundances of SiO_2 polymorphs (~40 vs. ~33%), lower total feldspar (~55 vs. ~66%), and higher secondary minerals (~6 vs. ~1%). The relatively large zeolite (stellerite) abundances reported by Vaniman et al. (especially in the lower lithophysal unit) were thought to be relatively unique to the repository horizon intersected by UE-25 UZ#16. Our identification of stellerite in three samples from the DST area is consistent with the findings of Vaniman et al. (1996), and suggests that stellerite in the Topopah Spring may be more widely distributed than previously thought. Other data for the Topopah Spring reported in Vaniman et al. (though not as densely sampled) are more similar to the data reported here (e.g., UE-25a#1 – SiO_2 polymorphs 34%, total feldspar 63%; UE-25p#1 – SiO_2 polymorphs 34%, total feldspar 64%; USW G-1 – SiO_2 polymorphs 33%, total feldspar 63%).

The average abundances for the internal corundum standard (Tables 1-3) are consistently larger than 20%, implying that we may not be identifying a phase(s) that comprises 3-9% of the sample by weight. However, a systematic error arising from a missed phase would tend to overestimate the abundances of all remaining phases, and this alone can not explain the differences between Vaniman et al. (1996) and our data. At least some of the differences between the data reported by Vaniman et al. and that reported here is probably due to differences between quantification by the

Rietveld method and the matrix flushing method. As mentioned in earlier reports (Viani and Roberts, 1996; Roberts and Viani, 1997a,b) and as discussed by Vaniman et al. (1996), there can be significant errors and difficulties associated with the matrix flushing method, especially for feldspars which display solid-solution behavior, and for samples with many overlapping peaks, such as the samples in question.

SiO$_2$ polymorphs

An important finding that has not been noted before, is the correlation between matrix color and SiO$_2$ mineralogy, and the negative correlation observed between cristobalite abundance and the sum of quartz plus tridymite (Figures 2 and 3). The negative correlation simply reflects the near uniformity in the abundance of total SiO$_2$ polymorph in these samples. Although the relationship is not quite inverse (the absolute value of the slopes of the best fit lines are less than unity), the negative correlation, and the correlation to matrix color discussed below, suggests that differing degrees of alteration of cristobalite (and possibly tridymite) to the more thermodynamically stable quartz has occurred in a more-or-less closed system.

As shown in Figure 3, the gray matrix zones adjacent to lithophysae and fractures have greater abundances of quartz and tridymite than samples of the purple or brown colored matrix. In almost all cases, gray matrix samples have higher quartz plus tridymite abundances than highly colored samples collected from the same drillcore (Table 2).

Tridymite abundance has been related to vapor phase precipitation on fracture and lithophysae surfaces (Vaniman et al., 1996), hence its greater abundance in the gray zones adjacent to fractures and lithophysal cavities is reasonable. However, tridymite was also identified in the more highly colored matrix zones that are apparently not adjacent to macroscopic fractures or lithophysae. As noted by Vaniman et al. (1996), microscopic fractures may be the source of tridymite in zones not adjacent to readily observable fractures or lithophysae.

These data suggest that alteration of cristobalite to quartz may have been favored in the zones adjacent to fluid pathways (i.e., interconnecting fractures and lithophysae) and may support the hypothesis that liquid water is necessary for the conversion of cristobalite to more stable phases (e.g., Ernst and Calvert, 1969). Whether the increased tridymite abundances in the gray matrix zones reflect vapor phase deposition at the time of devitrification, or subsequent aqueous phase alteration of cristobalite to a more stable phase, cannot be ascertained without supporting textural evidence.

Color differences of the matrix have been explained as differences in the distribution of hematite; more highly colored zones (brown and purple) are characterized by

6

small quantities of finely disseminated hematite, gray zones by hematite that is more localized (e.g., as fracture lining minerals), or as zones from which hematite has been depleted. The relationship between hematite distribution and SiO_2 mineralogy, if any, cannot be assessed from the data in this report. However, if hematite redistribution in the matrix is a result of post devitrification fluid flow regimes, then perhaps hematite redistribution and alteration of cristobalite to quartz occurred in response to the same flow events.

Fracture minerals

The cavity and fracture fill samples were hand picked out of the core sections to obtain specific phases for X-ray analysis. The representative phases include lithophysae cavity fill crystals, breccia fill crystals, black lathe-like crystals, and two matrix material samples. Two matrix types were also analyzed qualitatively; a purple matrix sample, and a conglomerate matrix sample exhibiting all three color variations. The results of these analyses are shown in Table 4. The diffraction patterns yielded relatively pure quartz for the lithophysae cavity fillings from boreholes CHE-1,5,6, and 10, and quartz with minor tridymite in the samples from boreholes CHE-5 and 6. One lithophysae fracture fill sample (CHE-1, 66.6-67.3) yielded quartz with minor feldspars, due to inclusion of some of the surrounding matrix in the sample. Sample CHE-1,122.6-123.2 yielded coexisting calcite and quartz. Breccia fill samples from boreholes CHE-2 and CHE-10 yielded large (~0.5cm square) crystals, determined to be calcite. A relatively large single crystal of hematite was identified in CHE-1. A manganese oxide phase (pyrolusite) was tentatively identified in CHE-10; the mass of material isolated was very small, and the diffraction pattern obtained yielded poor peak intensities. The conglomerate matrix sample was composed of cristobalite, quartz, feldspars, and a minor amount of smectite. The purple matrix sample contained cristobalite as the silica phase, with feldspars and a minor amount of smectite.

Conclusions

X-ray analysis of samples of Topopah Spring tuff has shown, in agreement with previous work, the uniformity of the total SiO_2 polymorph and feldspar abundances in the repository horizon. Within the repository horizon and adjacent zones of the Topopah Spring member, the relative abundance of quartz plus tridymite is positively correlated with gray altered zones adjacent to lithophysae and fractures. The relative abundance of cristobalite relative to quartz plus tridymite could potentially be used to assess the density of paleo fluid pathways. A strong negative correlation between cristobalite and quartz plus tridymite abundances may reflect post-devitrification alteration by aqueous fluids.

References

Chung, F.H. 1974. Quantitative interpretation of x-ray diffraction patterns of mixtures. I. Matrix-flushing method for quantitative multicomponent analysis. *J. Appl. Cryst.* 7: 519-525.

Ernst, W.G., and Calvert, S.E. 1969. An experimental study of the recrystallization of porcelanite and its bearing on the origin of some bedded cherts: Amer. Jour. Sci., 267A:114-133.

Roberts, S.K., and Viani, B.E., 1997a. *Mineral Abundances for Samples from Six Chemistry (Seamist) Boreholes in the Drift Scale Area (DST) of the ESF,* Yucca Mountain Project Milestone SP9510M4, Lawrence Livermore National Laboratory, February 28, 1997.

Roberts, S.K., and Viani, B.E. 1997b. *Mineral Abundances For Samples from Instrumentation Boreholes in the Access Drift Scale Test Area (DST) Of The ESF* Yucca Mountain Project Milestone Report SP9511M4, Lawrence Livermore National Laboratory, May 30, 1997

Schuraytz, B.C, Vogel, T.Z, and Younker, L.W. 1986. *Geochemical Gradients in the Topopah Spring Member of the Paintbrush Tuff: Evidence for Eruption Across a Magnetic Interface.* Lawrence Livermore National Laboratory, Livermore, CA. UCRL-53698.

Snyder, R.L., and Bish, D.L. 1989. Quantitative analysis. *In.* Bish, D.L., and Post, J.E. (eds.) *Modern Powder Diffraction.* Pp. 101-144. Reviews in Mineralogy, Mineralogical Society of America, Washington DC.

Vaniman, D.T., Bish, D.L., Chipera, S.J., Carlos, B.A., and Guthrie, Jr., G.D. 1996. *Summary and Synthesis Report on Mineralogy and Petrology Studies for the Yucca Mountain Site Characterization Project. Volume I. Chemistry and Mineralogy of the Transport Environment at Yucca Mountain* M0L.19961230.0037. Yucca Mountain Project Milestone 3665. Los Alamos National Laboratory, Los Alamos, NM.

Viani, B.E., and Roberts, S.K. 1996. *Determination of Mineral Abundances in Core Samples From the Exploratory Studies Facility Using Xray Diffraction.* Analysis report supporting Yucca Mountain Project TDIF# 305632; Mineral Abundances for Ten Samples From the Thermal Area of the ESF.

Young, R.A., 1993. Introduction to the Rietveld method. In Young, R.A. (ed). *The Rietveld Method,* p.1-38. IUCr Monographs on Crystallography 5, Oxford University Press, New York.

Table 1. Normalized mineral abundances[1] (weight-%) for samples from the Exploratory Studies Facility: Thermal test specimens from the SHT
        (Re-analyzed data originally reported in Viani and Roberts (1996))

Sample #	quartz	cristobalite	tridymite	albite	sanidine	clinoptilolite	smectite	muscovite
BJ-1-1.0-B	10	22		26	39		tr[2]	3
BJ-1-10.0-B	9	22		25	42		tr	
BJ-1-18.0-B	8	22		28	41		tr	
BJ-1-18.0-B	6	22		27	42		1	
MPBX-2-8.6-D	6	25		23	41		1	3
MPBX-3-12.5-B	9	20		24	42	3	tr	
MPBX-3-12.5-B	13	21		19	42	4	tr	
MPBX-4-5.0-B	2	28		28	41		tr	
H1-0.6-C	8	20		27	42	1	tr	
H1-11.3-C	8	24		25	42		tr	
H1-11.6-C	8	22		29	39		tr	
H1-22.2-B	8	23		22	46		tr	
H1-22.2-B	7	24		25	42		1	

[1] Normalized on corundum free basis (totals may not sum to 100 due to round-off error). Average corundum abundance 21.3±0.5. Average normalized abundances: total SiO_2 polymorphs – 30.5±1.7; total feldspars – 66.8±2.4; albite – 25.2±2.8; sanidine – 41.6±1.7.
[2] tr – the phase was identified in the XRD pattern, but Siroquant Rietveld analysis refined the abundance to zero.

Table 2. Normalized mineral abundances[1] (weight-%) for samples from the Exploratory Studies Facility: Samples collected from DST drill core
(Re-analyzed data originally reported in Roberts and Viani (1997a), and new data not previously reported).

DST Borehole #, depth interval	quartz	cristobalite	tridymite	albite	sanidine	zeolite[2]	smectite	sample color
CHE-1, 32.0-32.8	2	29		27	43			purple
CHE-1, 53.4-54.2	11	23		27	40			brown
CHE-1, 53.4-54.2	17	13	7	28	36			gray
CHE-1, 66.6-67.3	10	21		28	42			gray
CHE-1, 76.7-77.6	33	3	7	28	29			gray
CHE-1, 76.7-77.6	8	24		24	44			brown
CHE-1, 85.7-86.6	16	5	7	33	38			gray
CHE-1, 85.7-86.6	6	23		33	38			brown
CHE-1, 122.6-123.2	5	26		31	38			brown
CHE-2, 18.4-19.1	8	22		24	45		tr[3]	brown
CHE-2, 50.3-51.0	16	17		28	38		tr	brown
CHE-2, 65.0-65.7	10	17	10	25	38			gray
CHE-2, 76.7-77.4	4	25		29	43		tr	purple
CHE-2, 89.0-89.7	3	30		27	40			purple
CHE-2, 97.0-97.7	4	24	10	30	33			dark purple
CHE-2, 114.0-114.7	20	13		29	37			brown
CHE-2, 114.0-114.7	23	14		29	34			gray
CHE-2, 128.9-129.6	17	8	13	24	39			gray
CHE-2, 128.9-129.6	9	17	2	34	38		tr	brown
CHE-5, 5.2-6.0	14	19		31	37			brown
CHE-5, 5.2-6.0	19	8		33	40			gray

Table 2. Normalized mineral abundances[1] (weight-%) for samples from the Exploratory Studies Facility: Samples collected fron DST drill core
(Re-analyzed data originally reported in Roberts and Viani (1997a), and new data not previously reported).

DST Borehole #, depth interval	quartz	cristobalite	tridymite	albite	sanidine	zeolite[2]	smectite	sample color
CHE-5, 50.0-50.7	15	6	10	30	40			gray
CHE-5, 50.0-50.7	6	26		26	42		tr	brown
CHE-5, 74.2-74.9	8	24		25	43			brown
CHE-5, 74.2-74.9	12	12	14	25	38			gray
CHE-5, 74.2-74.9	11	11	12	26	39			gray
CHE-5, 74.2-74.9	4	23	8	31	35			dark
CHE-5, 82.8-83.5	17	13	4	30	36			matrix
CHE-5, 99.0-99.6	13	11		25	45	5 (st)		gray
CHE-5, 99.0-99.6	20	10	5	29	36			purple
CHE-6, 29.0-29.7	7	23	4	28	37			brown
CHE-6, 29.0-29.7	14	9	12	27	37			gray
CHE-6, 63.9-64.6	5	23	7	32	34			matrix
CHE-6, 74.8-75.5	5	27		28	40			purple
CHE-6, 74.8-75.5	15	19		27	39			brown
CHE-6, 74.8-75.5	8	16	9	29	38			gray
CHE-6, 74.8-75.5	4	18	3	47	28			purple
CHE-6, 74.8-75.5	7	11	14	26	41			gray
CHE-6, 91.3-92.0	7	22	5	30	35			brown
CHE-6, 99.7-100.4	5	25	5	28	37			brown
CHE-6, 99.7-100.4	5	25	5	28	37			brown
CHE-6, 99.7-100.4	18	19		25	38			gray
CHE-6, 105.0-105.5	7	26		28	39			brown

Table 2. Normalized mineral abundances[1] (weight-%) for samples from the Exploratory Studies Facility: Samples collected fron DST drill core
(Re-analyzed data originally reported in Roberts and Viani (1997a), and new data not previously reported).

DST Borehole #, depth interval	quartz	cristobalite	tridymite	albite	sanidine	zeolite[2]	smectite	sample color
CHE-6, 105.0-105.5	10	6	16	35	33			gray
CHE-6, 118.6-119.3	7	25		30	37			brown
CHE-6, 118.6-119.3	12	9	17	31	31			gray
CHE-7, 80.0-80.7	2	28	5	26	39			purple
CHE-7, 95.6-96.3	24	11	10	23	32			gray
CHE-7, 95.6-96.3	3	24	7	32	33			dark
CHE-7, 101.0-101.7	3	25	8	30	34			purple
CHE-7, 101.0-101.7	16	11	14	21	35	4 (cl)	tr	gray
CHE-10, 27.3-28.0	16	10		28	45			light brown
CHE-10, 27.3-28.0	10	20	3	22	45			brown
CHE-10, 75.6-76.3	7	25		28	40			brown
CHE-10, 75.6-76.3	10	7	16	32	35			gray
CHE-10, 75.6-76.3	8	19	6	30	38			matrix
CHE-10, 80.7-81.4	5	12	3	26	43	12 (st)	tr	dark
CHE-10, 85.0-85.7	17	6	12	30	35			gray
CHE-10, 85.0-85.7	25	9	2	31	33			dark
CHE-10, 100.1-101.0	21	6	10	29	35			gray
CHE-10, 100.1-101.0	24	6	4	34	32			dark

[1] Normalized on corundum free basis (totals may not sum to 100 due to round-off error). Average corundum abundance 20.6±1.7.Average normalized abundances: total SiO_2 polymorphs – 32.7±4.2; total feldspars – 67.1±4.1; albite – 27.9±2.9; sanidine – 39.2±4.1
[2] (cl) = clinoptilolite; (st) = stellerite
[3] tr – the phase was identified in the XRD pattern, but Siroquant Rietveld analysis refined the abundance to zero.

Table 3. Normalized mineral abundances[1] (weight-%) for samples from the Exploratory Studies Facility: Thermal test specimens from DST
     (Re-analyzed data originally reported in Roberts and Viani, 1997b).

Sample #	quartz	cristobalite	tridymite	albite	sanidine	zeolite[2]
SDM-MPBX1-1.0-1.2-D	11	23		23	43	
SDM-MPBX1-21.0-21.2-D	7	25	4	16	47	
SDM-MPBX1-21.0-21.2-D dup	8	24	6	18	45	
SDM-MPBX1-31.9-32.1-D	3	31		21	45	
SDM-MPBX1-40.4-40.6-D	17	17	8	17	41	
SDM-MPBX1-62.0-D	9	25		22	44	
SDM-MPBX1-80.7-80.9-D	10	24		20	46	
SDM-MPBX2-29.0-29.2-D	3	28		23	45	
SDM-MPBX2-29.0-29.2-D dup	3	29		27	42	
SDM-MPBX2-48.6-D	15	19		21	45	
SDM-MPBX2-72.0-D	5	29		22	44	
SDM-MPBX2-85.0-D	6	27		24	43	
SDM-MPBX3-17.5-17.7-D	7	26		24	43	
SDM-MPBX3-38.5-38.7-D	4	30		21	45	
SDM-MPBX3-85.6-D	9	23		18	47	3 (st)
AOD-HDFR#1-9.0-D	12	21		20	46	1 (cl)
AOD-HDFR#1-9.0-D dup	13	21		22	43	tr[3] (cl)
AOD-HDFR#1-48.5-D	9	24		21	46	
AOD-HDFR#1-68.6-D	11	24		21	44	
AOD-HDFR#1-98.0-D	36	3		23	39	

[1] Normalized on corundum free basis (totals may not sum to 100 due to round-off error). Average corundum abundance 22.0±0.8. Average normalized abundances: total SiO_2 polymorphs – 34.5±2.8; total feldspars – 65.4±2.8; albite – 21.4±3.1; sanidine – 44.1±1.7

[2] (cl) = clinoptilolite; (st) = stellerite

[3] tr – the phase was identified in the XRD pattern, but Siroquant Rietveld analysis refined the abundance to zero.

Table 4. Composition of cavity and fracture fill samples from the DST drill core samples.

Borehole #, depth int.	Sample type	Composition
CHE-1, 53.4-54.2	Lithophysae cavity filling	quartz
CHE-1, 66.6-67.3	Large lithophysae filling	quartz, minor feldspars[1]
CHE-1, 108.2-109.0	Single black crystal	hematite
CHE-1, 108.2-109.0	Conglomerate matrix	cristobalite, quartz, feldspars[1], trace of smectite
CHE-1,122.6-123.2	Coarse grained cavity filling	calcite + quartz
CHE-2, 50.3-51.0	Breccia fracture fill	calcite
CHE-2, 89.0-89.7	Fracture fill crystals	calcite
CHE-5, 99.0-99.6	Fracture fill crystals	quartz, minor tridymite
CHE-6, 63.9-64.6	Fracture fill crystals	quartz, minor tridymite
CHE-7, 80.0-80.7	Purple matrix	cristobalite, feldspars[1], trace of smectite
CHE-10, 27.3-28.0	Black crystals	manganese oxide
CHE-10, 27.3-28.0	Fracture fill crystals	quartz
CHE-10, 85.0-85.7	Shallow rim around lithophysae	quartz, cristobalite, feldspars[1], trace of smectite
CHE-10, 124.0-124.7	Large white vug crystal	calcite

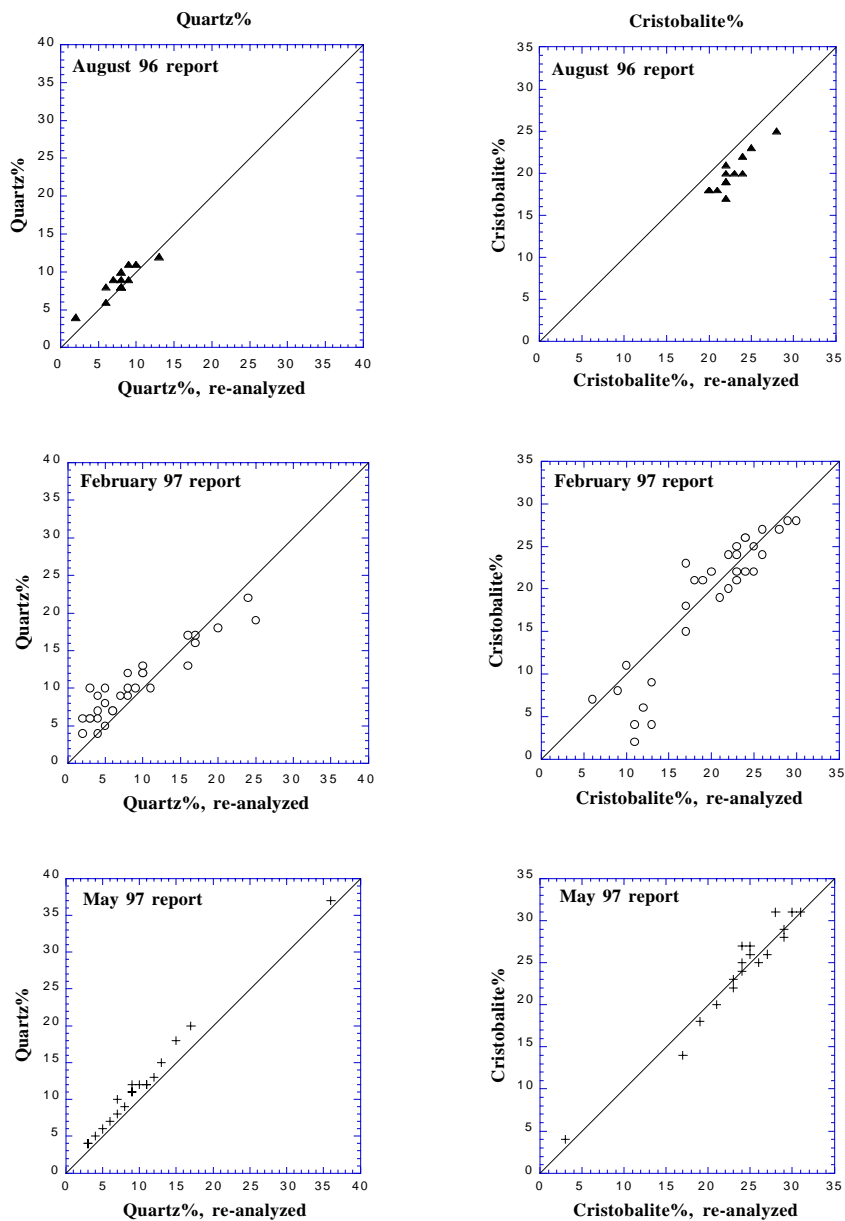(1) primarily albite and sanidine of varying composition

Figure 1. Comparison of normalized abundances of quartz and cristobalite determined using the matrix flushing method (August 96 and February 97 reports; Viani and Roberts, 1996; Roberts and Viani, 1997a) with normalized abundances re-analyzed using the Rietveld method (top and middle graphs). Lower graphs (May 97 report; Roberts and Viani, 1997b) compare normalized abundances of quartz and

15

cristobalite determined using initial and optimized Rietveld method parameters. Solid line represents 1:1 correspondence.
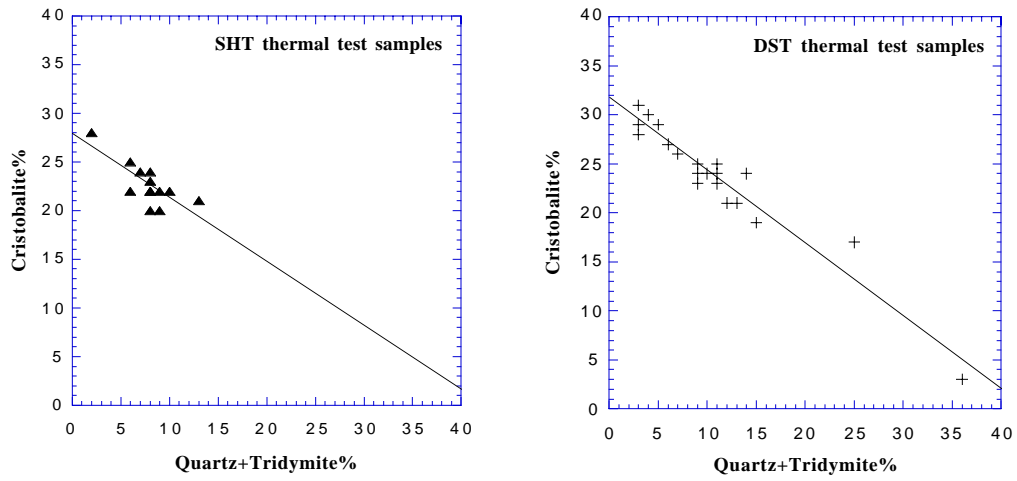
.

Figure 2. Variation in cristobalite abundance vs. quartz plus tridymite abundance for SHT and DST thermal test samples. Solid line is the best fit regression to the data.
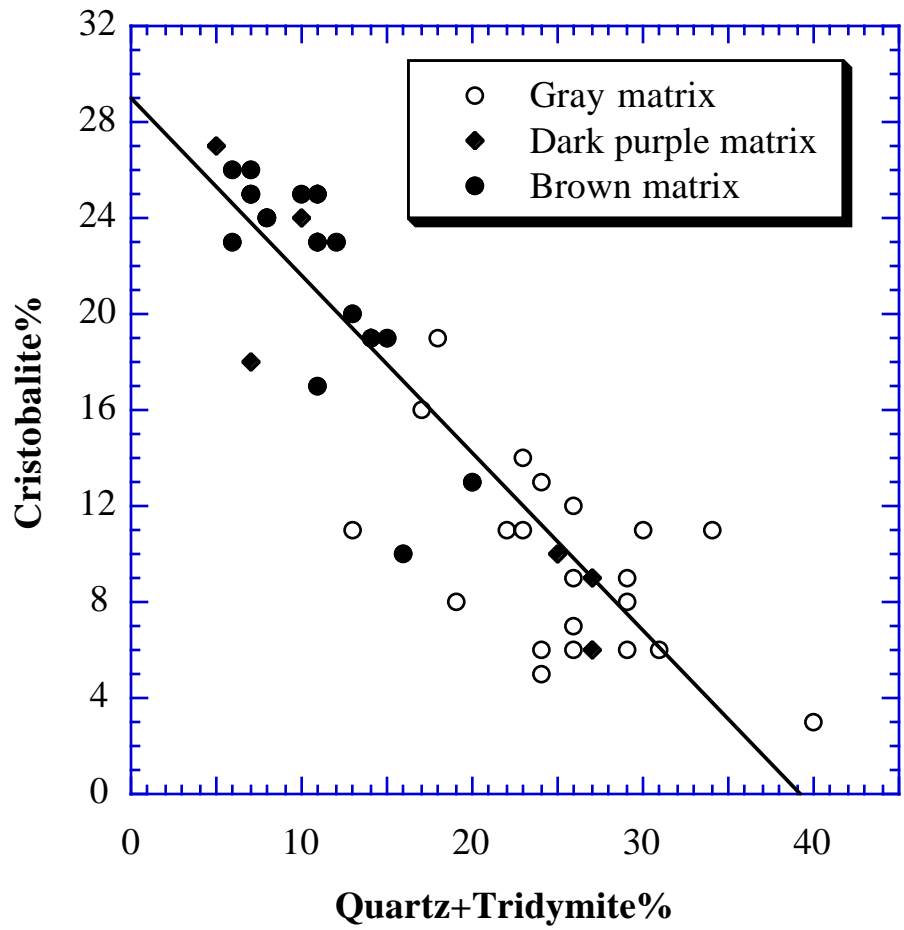
Figure 3. Variation in cristobalite abundance vs. quartz plus tridymite abundance for DST core samples of different matrix color collected from the same core. Solid line is the best fit regression to the data.